Specific and behaviourally consequential astrocyte G_q GPCR signaling attenuation *in vivo* with iβARK

Jun Nagai, Arash Bellafard, Zhe Qu, Xinzhu Yu, Matthias Ollivier, Mohitkumar R. Gangwani, Blanca Diaz-Castro, Giovanni Coppola, Sarah M Schumacher, Peyman Golshani, Viviana Gradinaru, Baljit S. Khakh

Correspondence: bkhakh@mednet.ucla.edu

Supplementary information

Figures S1-12
Movie S1: PE-evoked Ca^{2+} responses in striatal astrocytes expressing iβARK(D110A)
Movie S2: PE-evoked Ca^{2+} responses in striatal astrocytes expressing iβARK
Excel file S1: Details of statistical analyses, n numbers and relevant parameters (sheets 1-16; tabs colored in blue), as well as RNA-seq from striatal astrocytes expressing iβARK or iβARK(D110A) reporting raw FPKM values for input and IP (sheet 17; tab colored in red), complete gene list detected in IP and FDR values (sheet 18; tab colored in red), and raw data values of analysis shown in Figure 4B-D (sheet 19; tab colored in red)

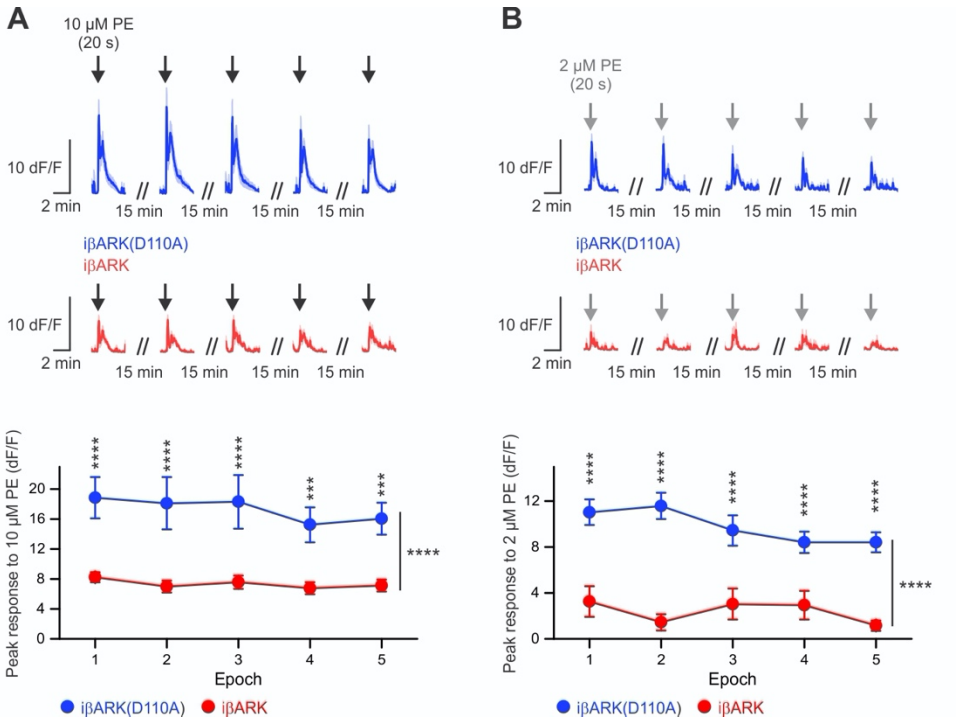

Figure S1. iβARK reduced Ca^{2+} responses induced by repetitive stimulation of endogenous G_q-coupled GPCRs (related figure 2). The Ca^{2+} responses to local application of phenylephrine (PE), an agonist of G_q-coupled α1-adrenergic receptors, at 10 (**A**) or 2 μM (**B**) in dorsal striatal (dSTR) astrocytes expressing iβARK(D110A) or iβARK. n = 12-13 astrocytes from 4 mice for each experimental configuration. Two-way repeated measures ANOVA was used. Full details of numbers, precise *P* values, and statistical tests are reported in Excel file S1. Average data are shown as mean ± SEM. In some cases, the SEM symbol is smaller than the symbol for the mean. NS, not significantly different. ***$P < 0.001$, ****$P < 0.0001$.

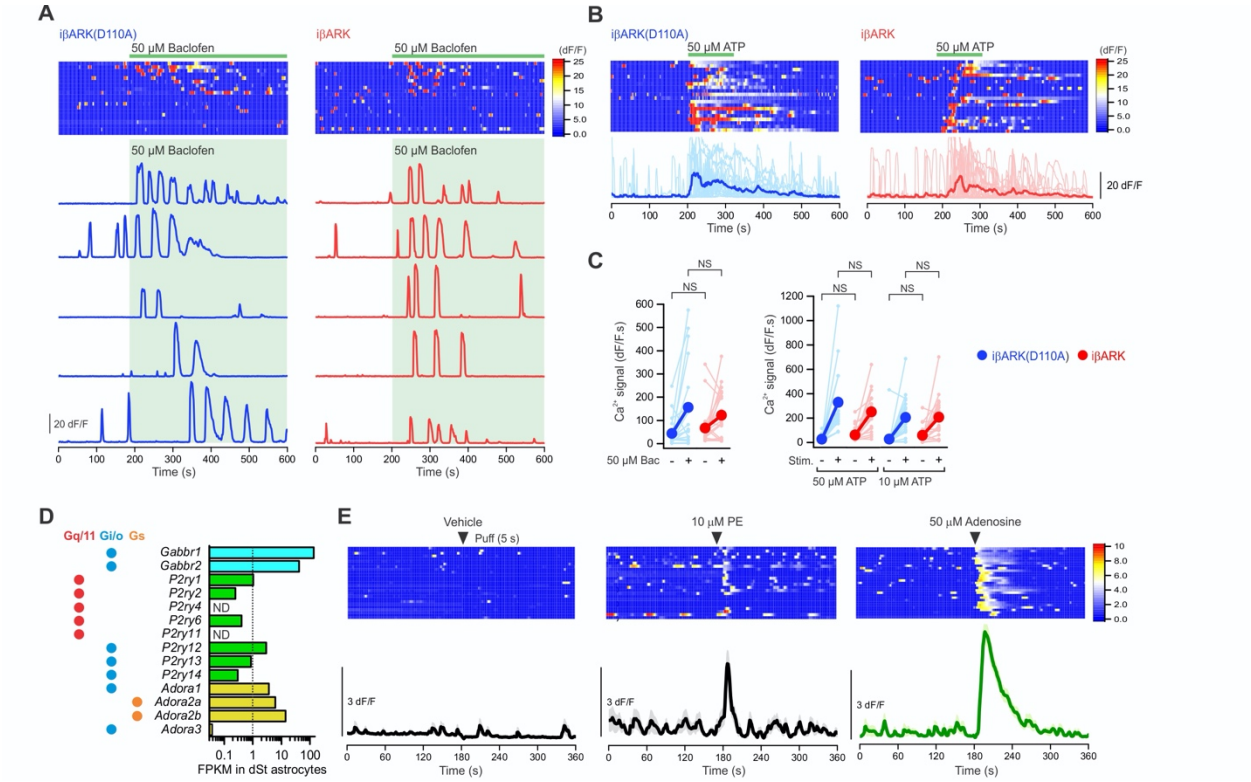

Figure S2. iβARK does not alter Ca^{2+} responses induced by endogenous G_i- and G_s-coupled GPCRs (related figure 2). (**A-B**) Kymographs and dF/F traces of Ca^{2+} responses in iβARK(D110A)- and iβARK-expressing dSTR astrocytes evoked by applications in bath of baclofen at 50 μM, an agoinst of $G_{i/o}$-coupled $GABA_B$ receptors (**A**), or ATP at 50 μM (**B**). TTX at 300 nM was applied in bath throughout the experiments. n = 20-22 astrocytes from 5-6 mice for each experimental configuration. (**C**) Summary plots for experiments related to **A-B**. Baclofen- and ATP-evoked Ca^{2+} responses were not reduced in dSTR astrocytes by iβARK. Nested one-way ANOVA was used. (**D**) The bar graph show FPKM values of RNA-seq data from dSTR astrocytes for $GABA_B$ receptors (light blue), P2Y receptors (green) and adenosine receptors (yellow). Color dots represent G-protein coupling of the receptors, indicating that dSTR astrocytes express G_q, G_i, G_s-coupled purinergic receptors. ND, not detected. (**E**) Kymographs and dF/F traces of Ca^{2+} responses in dSTR astrocytes evoked by 5 s puff applications of vehicle (17 astrocytes from 5 mice), phenylephrine (PE at 10 μM; 24 astrocytes from 4 mice) or adenosine (at 50 μM; 26 astrocytes from 6 mice). Full details of numbers, precise *P* values, and statistical tests are reported in Excel file S1. Average data are shown as mean ± SEM. In some cases, the SEM symbol is smaller than the symbol for the mean. NS, not significantly different.

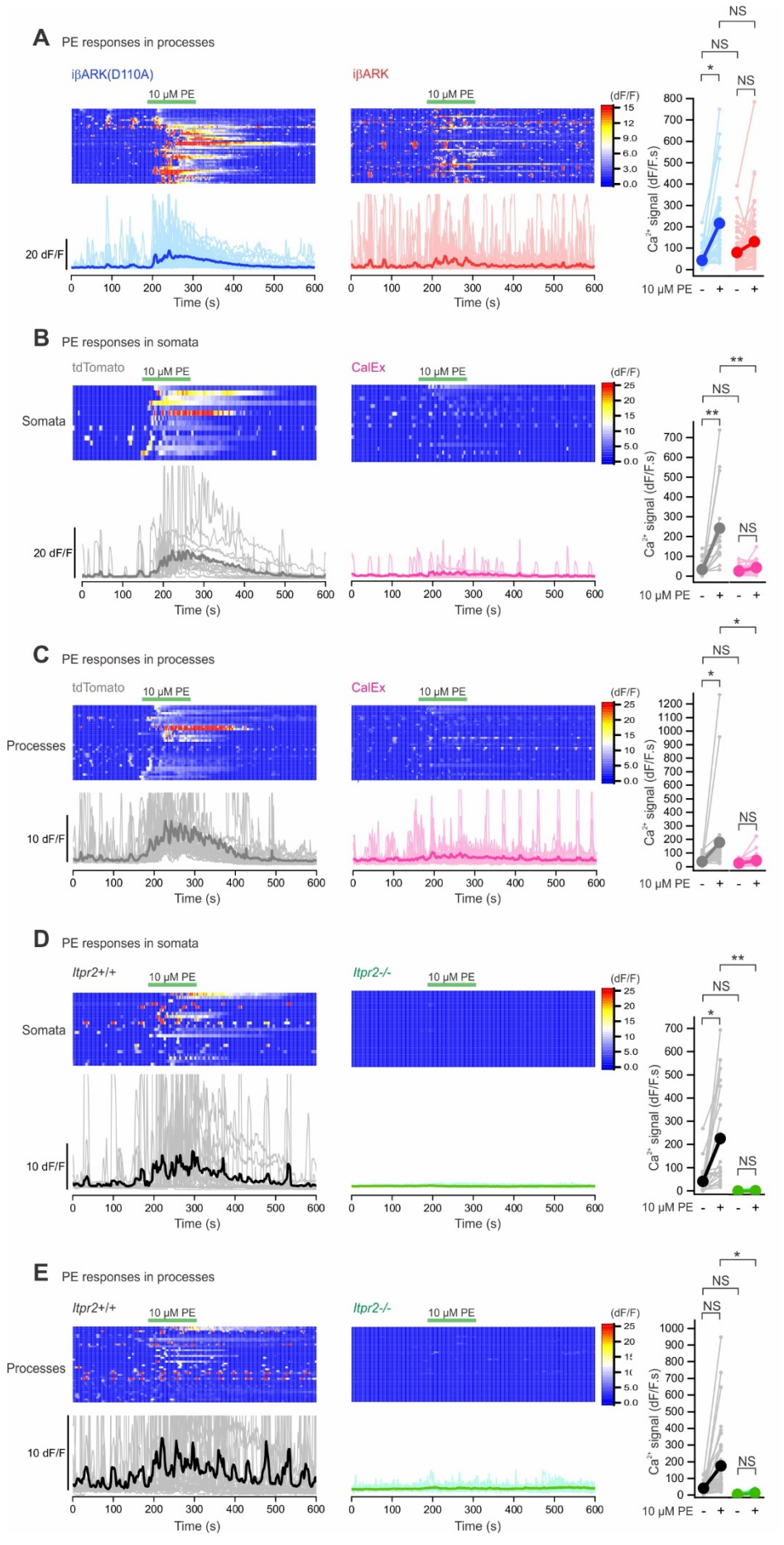
A
PE responses in processes
iβARK(D110A)
iβARK
10 μM PE
(dF/F)
20 dF/F
Time (s)
Ca2+ signal (dF/F.s)
NS
B
PE responses in somata
tdTomato
CalEx
Somata
C
PE responses in processes
Processes
10 dF/F
D
PE responses in somata
Itpr2+/+
Itpr2-/-
E
PE responses in processes

Figure S3. Reduced PE-evoked responses in astrocytes from IP$_3$R2 deletion and CalEx expressing mice (related figure 2 and 3). (**A**) Kymographs and dF/F traces of Ca^{2+} responses in dSTR astrocyte processes from iβARK(D110A)- and iβARK-expressing dSTR astrocytes evoked by applications in bath of PE at 10 μM. TTX at 300 nM was applied in bath throughout the experiments. (**B-C**) Kymographs and dF/F traces of Ca^{2+} responses in dSTR astrocyte somata and processes from wild-type (*Itpr2*$^{+/+}$) or IP$_3$R2 deletion (*Itpr2*$^{-/-}$) mice evoked by applications in bath of PE at 10 μM. The summary plots are shown in the right graph. No spontaneous nor evoked Ca^{2+} signaling was observed in *Itpr2*$^{-/-}$ astrocytes. n = 23-24 astrocytes from 5-6 mice for each experimental configuration. (**D-E**) Kymographs and dF/F traces of Ca^{2+} responses in dSTR striatal astrocyte somata and processes with virally expressed tdTomato (virus infection control) or CalEx evoked by applications in bath of PE (10 μM). The summary plots are shown in the right graph. PE-evoked responses were significantly reduced by CalEx relative tdTomato control. n = 15-20 astrocytes from 3-6 mice for each experimental configuration. Nested one-way ANOVA was used. Full details of numbers, precise *P* values, and statistical tests are reported in Excel file S1. Average data are shown as mean ± SEM. In some cases, the SEM symbol is smaller than the symbol for the mean. **P* < 0.05, ***P* < 0.01. NS, not significantly different.

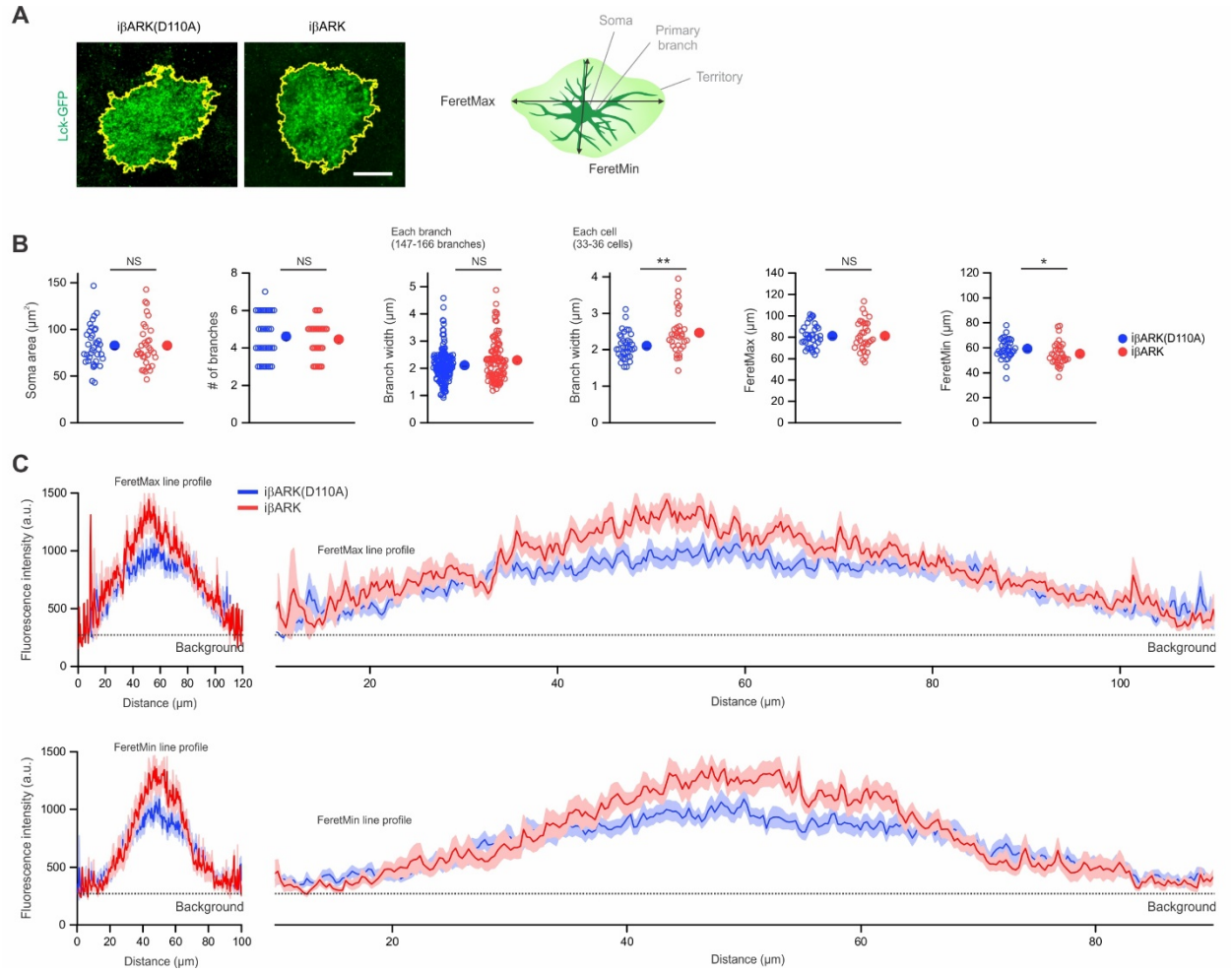

Figure S4. Morphology of dSTR astrocytes expressing iβARK(D110A) or iβARK (related figure 3). (**A**) Examples of two astrocytes from iβARK(D110A) and iβARK group and schematics of measured parameters of astrocyte morphology. (**B**) Comparison of soma area, the number and width of branches, Feret's diameters between groups. n = 33-36 astrocytes from 3 mice for each experimental configuration. Mann–Whitney U test was used. (**C**) Averaged fluorescence profiles of Lck-GFP (membrane tethered GFP) corresponding to lines of FeretMax (top) or FeretMin (bottom) diameter. The central peak of fluorescence reflects the brightest pixels in territory, mainly from surface of soma and primary branches. Full details of numbers, precise *P* values, and statistical tests are reported in Excel file S1. Average data are shown as mean ± SEM. In some cases, the SEM symbol is smaller than the symbol for the mean. **P* < 0.05, ***P* < 0.01. NS, not significantly different.

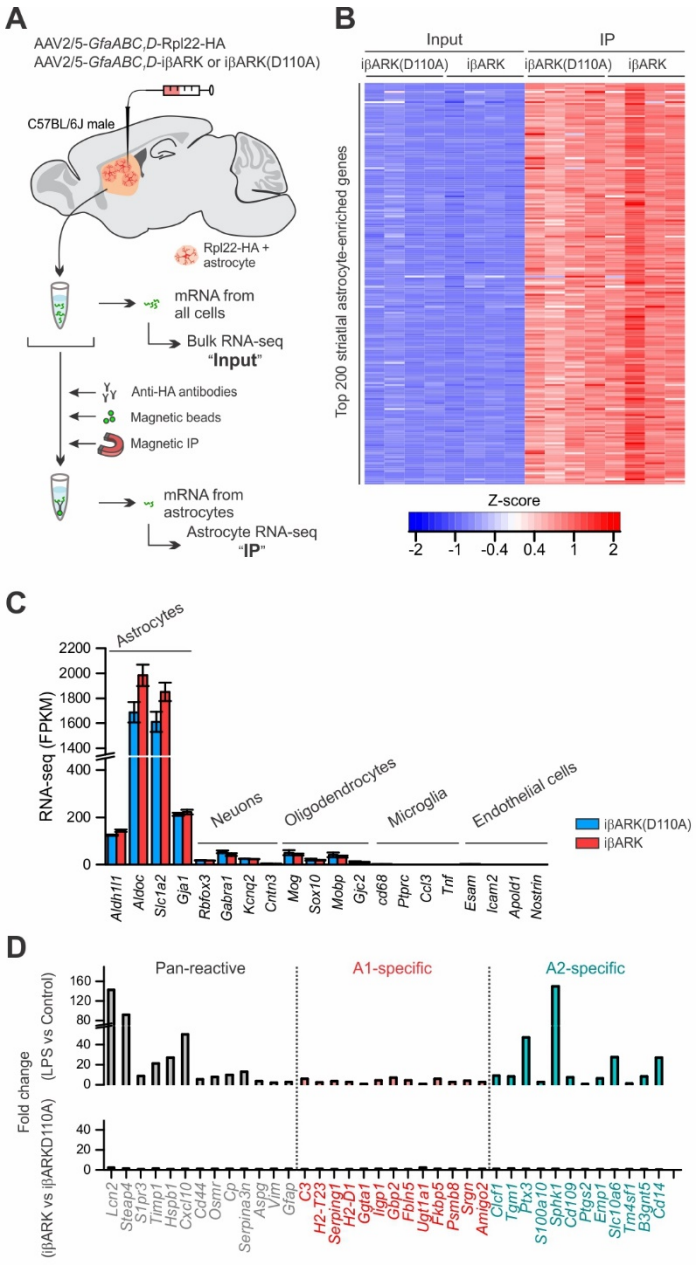

Figure S5. Little effect on transcriptomic profiles of dSTR astrocytes by iβARK (related figure 4). (**A**) Cartoon illustrating AAVs for selectively expressing Rpl22-HA and iβARK or iβARK(D110A) in astrocytes in dSTR via intracranial microinjections and the outline of the protocol for RNA-seq. (**B**) Heat map showing relative enrichment (red) or depletion (blue) of the top 200 adult striatal astrocyte markers. Results from sixteen RNA-seq samples for both input and IP from eight mice (four mice with iβARK(D110A) and four mice with iβARK in dSTR astrocytes) are shown. The row Z scores were calculated using the FPKM values. These data show that the RNA-seq data were replete with known astrocyte markers, which served to validate the approach. (**C**) Gene expression levels of cell-specific markers for astrocytes, neurons, oligodendrocytes, and microglia in IP samples from the iβARK(D110A) and iβARK groups. n = 4 mice per group. Data are shown as mean ± SEM. All the RNA-seq data are provided the Excel file S1. (**D**) Fold-change of pan-reactive, A1-, and A2-astrocyte-specific markers between iβARK IP and iβARK(D110A) IP samples. As a positive control, i.p. injection of LPS (5 mg/kg) was used.

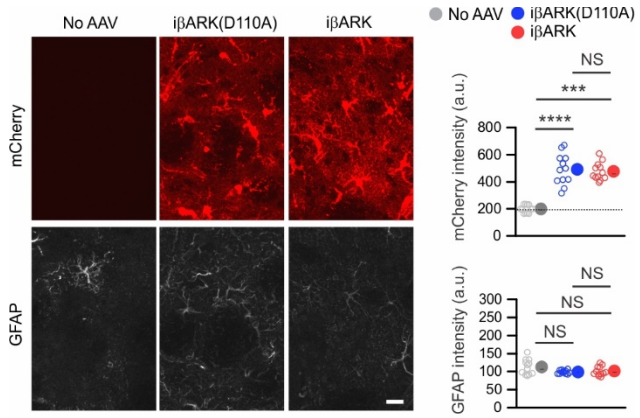

Figure S6. iβARK expression in dSTR astrocytes did not affect GFAP expression (related figure 4). Immunohistochemical analysis of GFAP expression in dSTR without and with AAV injections for expressing iβARK mCherry or iβARK(D110A) mCherry. No change in GFAP immunoreactivity was observed between groups. n = 12 FOVs from 3 mice per group. Nested one-way ANOVA was used. Scale bar: 20 μm. Full details of numbers, precise *P* values, and statistical tests are reported in Excel file S1. ***$P < 0.001$, ****$P < 0.001$. NS, not significantly different.

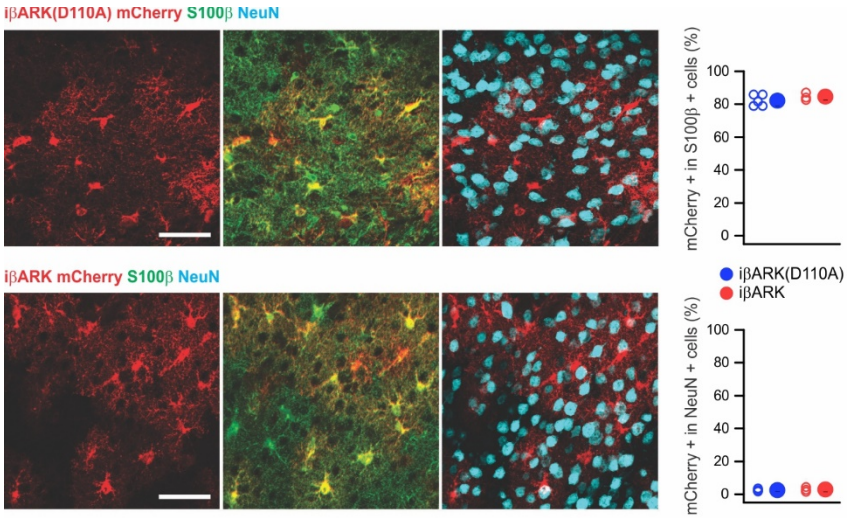

Figure S7. Astrocyte selective expression of iβARK in the visual cortex (related figure 5). The images show that intracranial AAV2/5-*GfaABC1D*-iβARK(D110A) mCherry or -iβARK mCherry microinjection resulted in iβARK expression in the visual cortex layer II/III with cell selectivity for astrocytes. S100β is a marker for astrocytes (green) and NeuN is a marker for neurons (blue). The scatter graph shows that ~82-85% of the S100β positive astrocytes were iβARK or iβARK(D110A) positive. Little expression in NeuN positive cells (~2.9%). n = 3 mice. Scale bars, 50 μm.

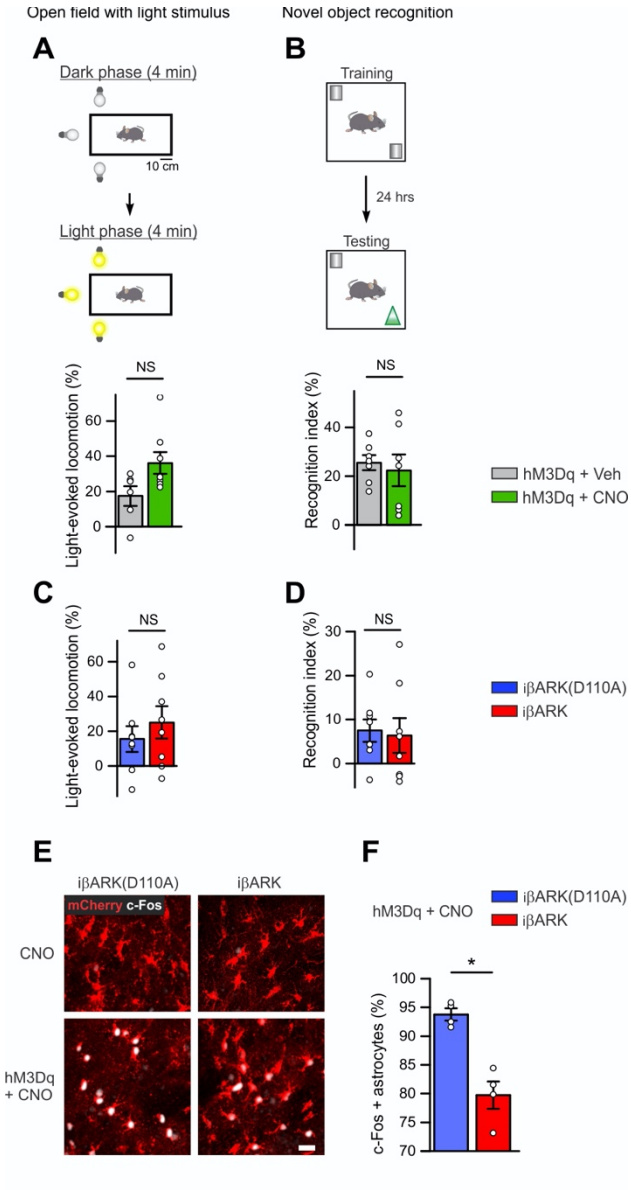

Figure S8. Additional assessments of *in vivo* consequences of iβARK expression and G_q-DREADD stimulation in dSTR astrocytes (related figure 6). (**A**) The cartoon illustrates the modified open field test with a light stimulus. In this initially dark open field, onset of a localized visual stimulus drives investigatory activity. The bar graphs show light stimulus-evoked changes in distance travelled by mice in the open field chamber. Increased ambulation in response to light simulation was observed both in the $hM3D_q$ + vehicle (Veh) group and $hM3D_q$ + CNO group. n = 8 mice per group. (**B**) The behavioral layout of the novel object recognition task. Both the $hM3D_q$ + Veh group and $hM3D_q$ + CNO group spent more time around the novel object. n = 8 mice per group. (**C**) Light-evoked increase in ambulation was observed both in the iβARK(D110A) and iβARK groups. n = 8 mice per group. (**D**) The iβARK(D110A) group and iβARK group showed similar performance in the novel object recognition task. n = 8 mice per group. Mann–Whitney U test was used. (**E-F**) *In vivo* $hM3D_q$ activation by CNO increased c-Fos expression in striatal astrocytes and such c-Fos activation was significantly reduced by iβARK. Mann–Whitney U test was used. n = 4 mice. Scale bar, 20 μm. Data are mean ± SEM. Full details of numbers, precise *P* values, and statistical tests are reported in Excel file S1. **P* < 0.05. NS, not significantly different.

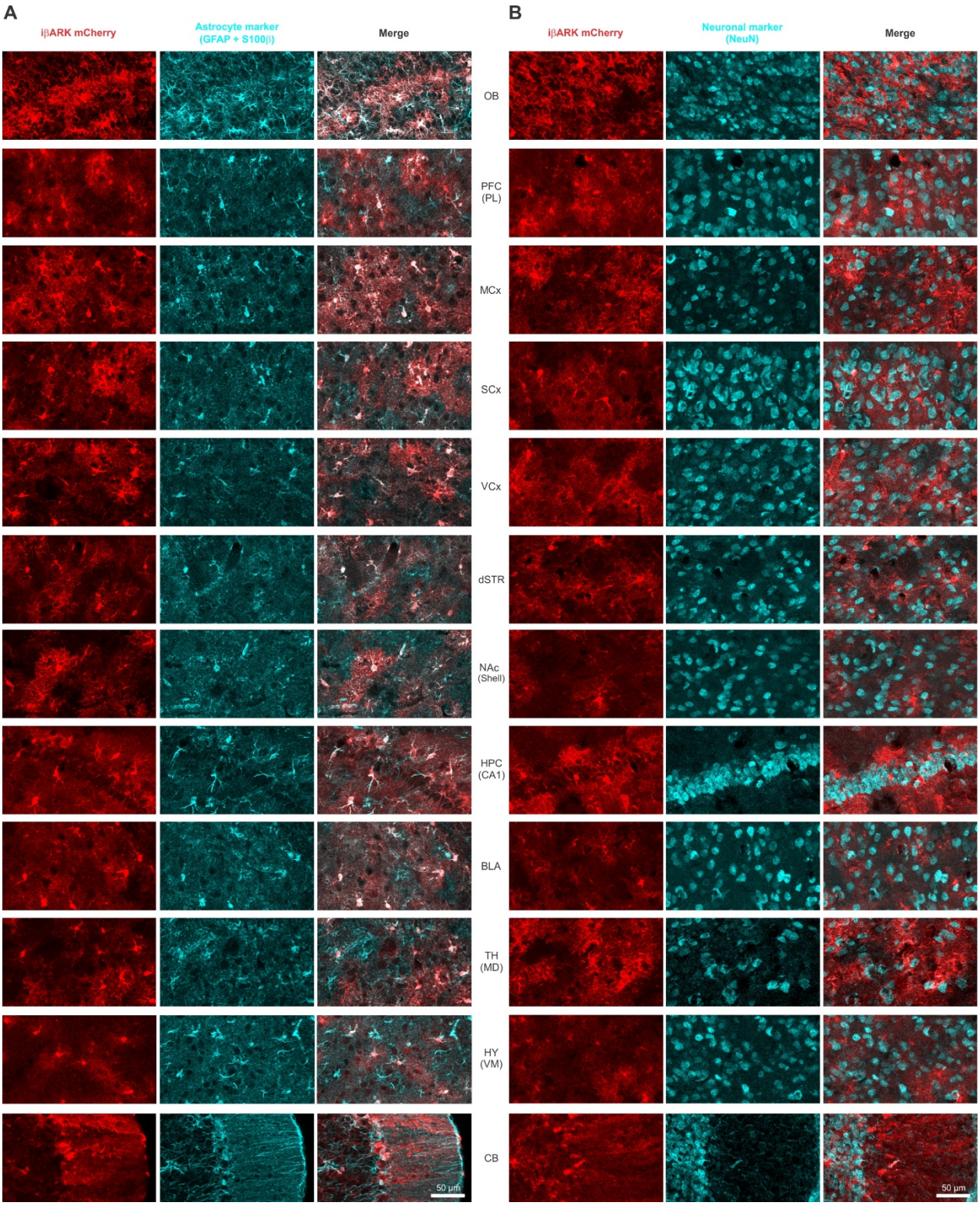

Figure S9. Representative images for PHP.eB AAV-based expression of iβARK mCherry in 12 brain regions (related figure 7). Representative staining of iβARK mCherry (red) imaged with astrocyte markers (GFAP + S100β; A) or neuronal marker (NeuN; B). Scale bars: 50 µm.

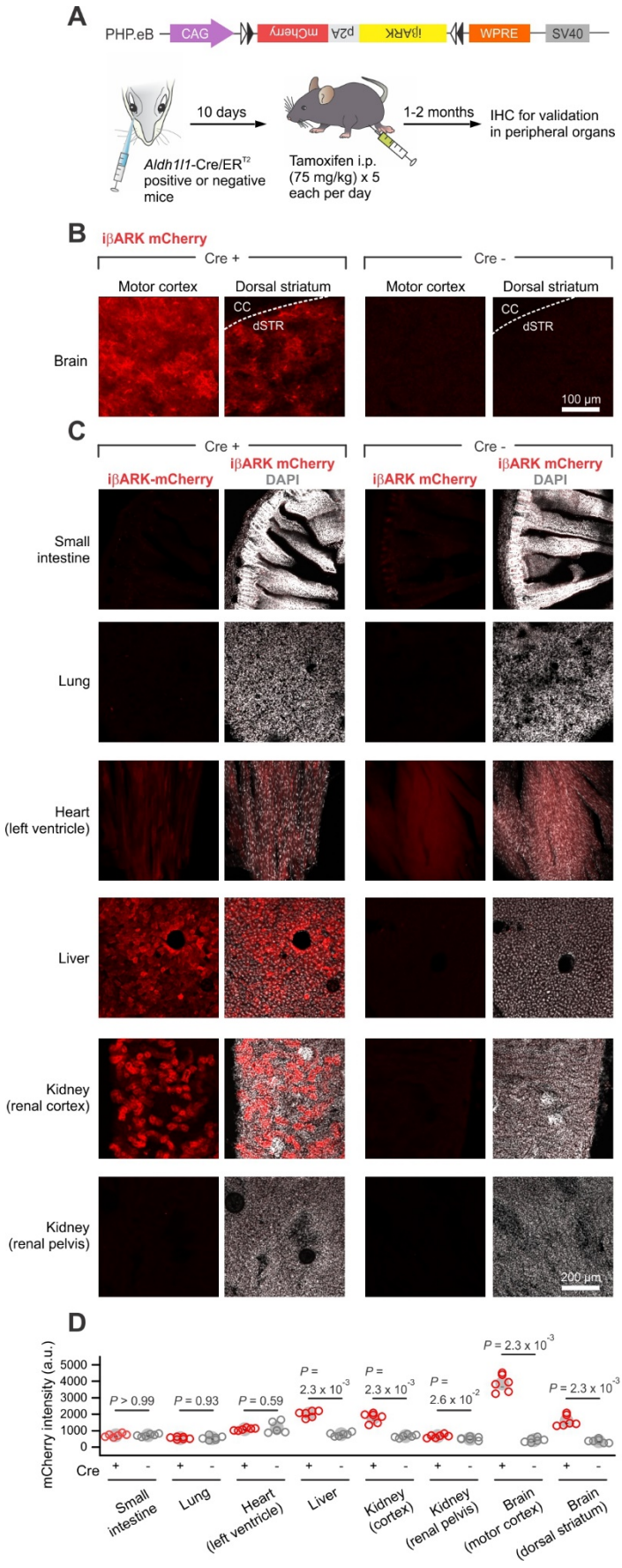

Figure S10. Assessment of AAV-PHP.eB-mediated iβARK expression in peripheral organs in *Aldh1l1*-Cre/ER^{T2} mice (related figure 7). (**A**) Cartoon illustrating a genome construct packaged by AAV-PHP.eB for Cre-dependent iβARK mCherry expression and its intravenous injection into *Aldh1l1*-Cre/ER^{T2} positive or negative mice. (**B**) Representative images of iβARK mCherry expression in the brain. iβARK mCherry signals were observed in the motor cortex and dSTR from Cre positive mice, but not in Cre negative mice. (**C**) Representative images of iβARK mCherry expression in indicated peripheral organs. In Cre negative mice, no iβARK mCherry signals were observed in any organ. In the small intestine, the lung, the left ventricle of heart and the renal pelvis of kidney from Cre positive mice, there were no significant iβARK mCherry signals, while significant expressions were observed in the liver and the cortex of kidney. (**D**) Summary plots for the expression of iβARK mCherry in peripheral organs and the brain. n = 6 slices from 3 mice per group. Mann–Whitney U test was used. Scale bars, 100 μm in **B** and 200 μm in **C**. Full details of numbers, precise *P* values, and statistical tests are reported in Excel file S1. Data are shown as mean ± SEM. In some cases, the SEM symbol is smaller than the symbol for the mean. **P* < 0.05, ***P* < 0.01. NS, not significantly different.

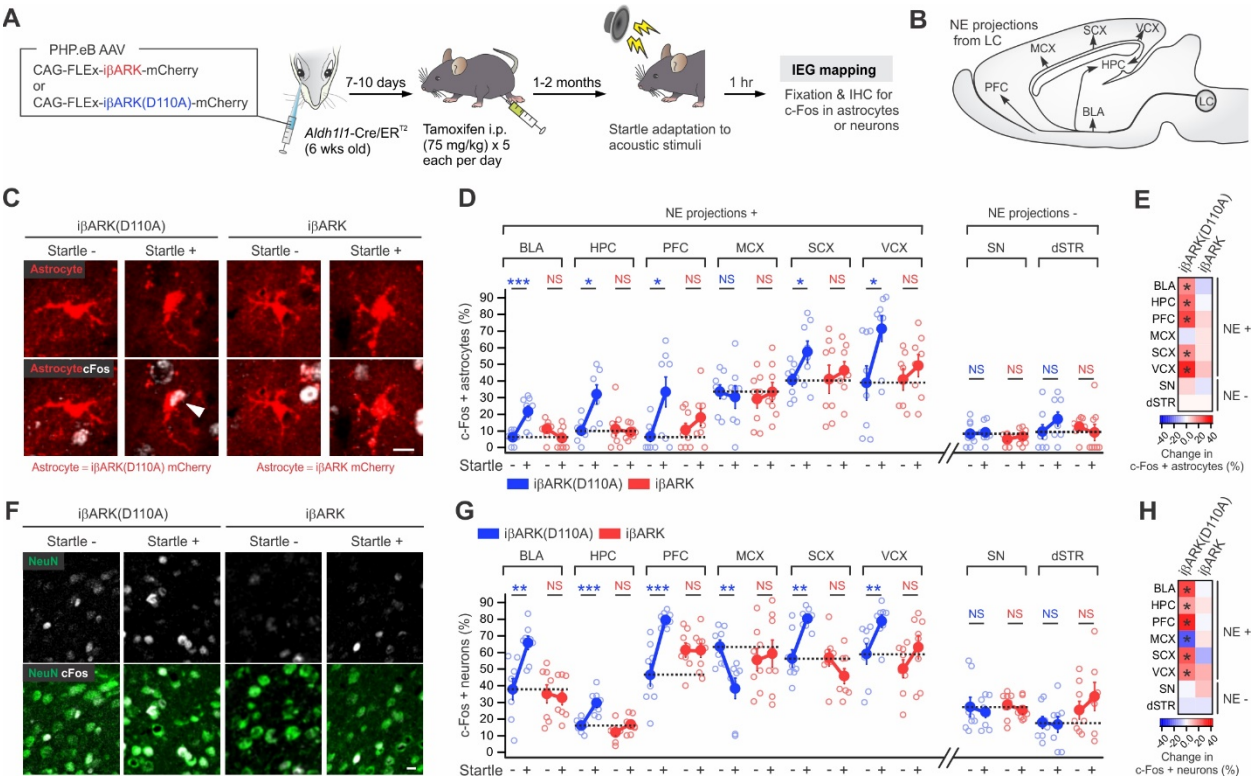

Figure S11. Attenuation of astrocyte G_q pathway blunted the startle adaptation-associated c-Fos mobilization in astrocytes and neurons (related figure 8). (**A**) Cartoon illustrating the approaches for attenuating astrocyte G_q pathway signaling in whole brain and assessing its cellular consequences. (**B**) Behavioral startle stimuli activates noradrenergic (NE) system including the locus coeruleus (LC) neurons that project mainly to the ipsilateral forebrain. The axons extensively branch out and have terminals in diverse remote brain regions such as the basolateral amygdala (BLA), hippocampal CA1 (HPC), prelimbic subregion of prefrontal cortex (PFC), motor cortex (MCX), sensory cortex (SCX) and visual cortex (VCX). The major region that does not receive input from the LC is the area that contains the basal ganglia including the dorsal striatum (dSTR) and substantia nigra (SN). (**C-E**) Assessment of c-Fos expression in astrocytes in multiple brain areas of the iβARK(D110A) and iβARK groups with and without startle stimuli (n = 7-8 slices from 4 mice per group). (**C**) Images show astrocytes in PFC from each group. The arrowhead indicates a c-Fos positive astrocytes. Significant upregulation of c-Fos in astrocytes was observed in the iβARK(D110A) group but not in the iβARK group in BLA, HPC, PFC, SCX and VCX. (**D**) The scatter graph summarizes the percentage of c-Fos-positive astrocytes in eight brain areas from the iβARK(D110A) group (blue) and the iβARK group (red) with and without startle stimuli. (**E**) Heat map summarizes the changes in c-Fos-positive astrocytes assessed in such experiments. Mann–Whitney U test was used. (**F-H**) Assessment of c-Fos expression in neurons in multiple brain areas in indicated 4 experimental groups. (**F**) Images show that c-Fos in neurons of prelimbic PFC was significantly upregulated in the iβARK(D110A) group but not in the iβARK group. (**G**) The scatter graph summarize the percentage of c-Fos-positive neurons in eight brain areas in indicated 4 experimental groups. (**H**) Heat map summarizes the changes in c-Fos positive neurons assessed in such experiments. Mann–Whitney U test was used. Scale bars, 10 μm in **c** and 20 μm in **F**. Full details of numbers, precise *P* values, and statistical tests are reported in Excel file S1.

Average data are shown as mean ± SEM. In some cases, the SEM symbol is smaller than the symbol for the mean. *$P < 0.05$, **$P < 0.01$, ***$P < 0.001$. NS, not significantly different.

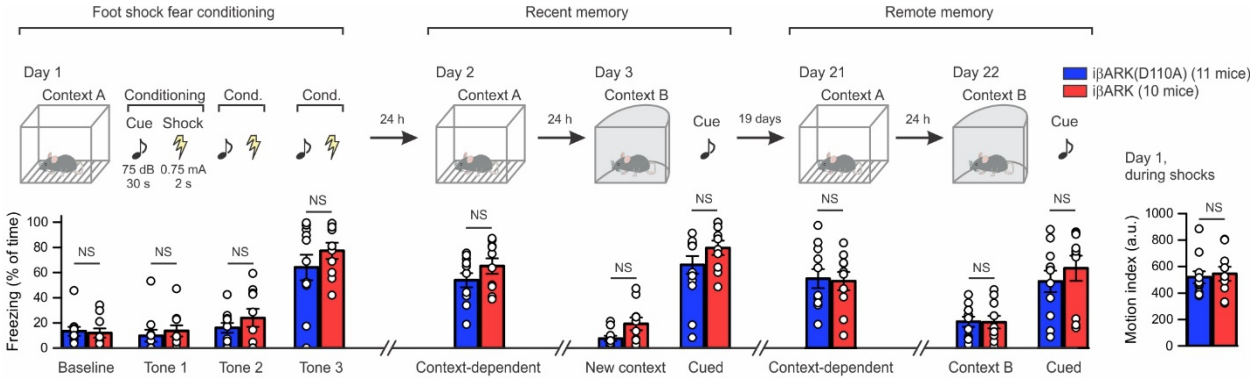

Figure S12. Additional assessments of the behavioral consequences of brain-wide attenuation of astrocyte G_q pathway (related figure 8). Fear conditioning memory test. Top, cartoon illustrating the experimental paradigms of conditioning of aversive foot shock (0.75 mA, 2 s) with the context A and the tone auditory cue (75 dB, 30s) that was given just prior to the shocks (day 1) and the testing for recent contextual fear memory (day 2), recent cue-dependent fear memory (day 3), remote contextual fear memory (day 21), and remote cue-dependent fear memory (day 22). Bottom graphs are freezing responses of mice (n = 11 mice in the iβARK(D110A) group and 10 mice in the iβARK group). iβARK did not alter any performance in these tests, suggesting no alteration in contextual and cued fear memory. The graph on the right shows that the iβARK(D110A) group and the iβARK group display similar motor responses to foot shocks on day 1, indicating no difference in sensorimotor gating, which is consistent with the data shown in **Figures 8B,C,E**. Mann–Whitney U test was used. Full details of numbers, precise *P* values, and statistical tests are reported in Excel file S1. Average data are shown as mean ± SEM. NS, not significantly different.